## POLITECNICO DI TORINO
## Repository ISTITUZIONALE

Glass-based sealants for joining  to ''-Al2O3 in Na–Zn batteries

(Article begins on next page)

01 September 2025

# Glass-based sealants for joining α to β''-Al$_2$O$_3$ in Na–Zn batteries

F. D'Isanto [a,*], A. Baggio [a], M. Salvo [a], D. Basso [b], D. Gaia [b], F. Smeacetto [a]

[a] *Politecnico di Torino, Department of Applied Science and Technology, Corso Duca degli Abruzzi 24, 10129, Torino, Italy*
[b] *FZSoNick S.A., Via Laveggio 15, 6855, Stabio, Switzerland*

## ARTICLE INFO

## ABSTRACT

This study deals with the design and the characterisation of glass-based materials for the hermetic sealing of ceramic components (α-to β''-Al$_2$O$_3$) in solid-electrolyte cells operating at approximately 300 °C. A silica-based commercially available glass and a newly developed silica-free glass, potentially resistant to corrosion by molten sodium salts, are reviewed and discussed. 25 wt% alumina powder is incorporated into both formulations. The sintering behaviour of the glass systems and their wetting characteristics on alumina are evaluated at the selected sealing temperatures: 900 °C for 40 min (for the silica-based system) and 700 °C for 1 h (for the silica-free system). The viscosity of both glass systems at these temperatures, which is approximately 10$^5$ Poise, is deemed suitable for facilitating proper glass flow and bonding with the alumina components. Furthermore, the coefficient of thermal expansion (CTE) of the potential sealant candidates is investigated. The results demonstrate good compatibility between the glass-based systems (CTE ≈ 7–7.6· 10$^{-6}$ K$^{-1}$ at temperatures ranging from 100 to 300 °C) and α- and β''-Al$_2$O$_3$ (CTE ≈ 7.3· 10$^{-6}$ K$^{-1}$ within the same temperature range). The microstructural analysis conducted using field-emission scanning electron microscopy (FE-SEM) confirms good thermo-mechanical matching between the glass-based sealants and the alumina ceramic components and that no reaction occurs during the sealing between alumina powder and the glass matrix.

## 1. Introduction

The increasing amount of electricity consumed in everyday life, its high cost and the environmental impact of fossil fuels are guiding research for efficient and sustainable energy devices, which can store energy and convert it for utility-scale energy-storage applications [1]. Due to their high energy and power density, rechargeable sodium-nickel chloride batteries, also known as ZEBRA batteries (Zero Emission Battery Research Activities), are one of the best solutions for the intermediate-temperature (250–300 °C) energy storage demand for stationary applications and electric and hybrid cars [2–4]. This technology uses a metal-based cathode and a molten sodium anode to provide exceptionally safe and reliable power generation for low-cost stationary storage. Recyclability, zero gas emission, and negligible fire risk make ZEBRA batteries one of the best choices for the oil & gas industry, renewable power generation, transmission and distribution of energy, communications, railways and other industrial uses [4,5].

In general, this type of battery is based on electrochemical charge/discharge reactions that occur between a positive electrode (cathode) consisting mainly of nickel (Ni) and sodium chloride (NaCl) and a negative electrode (anode) that typically consists of molten sodium (Na). The electrolyte is NaAlCl$_4$, liquid at the operating temperature of the cell, and a ceramic separator (β''-alumina) provides fast transport of sodium ions and ensures the galvanic insulation between anode and cathode [2,5].

Recently, a similar ZEBRA battery set-up has been proposed and studied; it uses Na and Zn for electrode materials, operating as a Na–ZnCl$_2$ battery instead of a Na–NiCl$_2$ one, with a significant cost reduction due to the replacement of nickel with zinc, which is cheaper and more abundant [6]. This new approach was already studied in high-temperature all-liquid cells [7,8].

Hermetic sealing to join active β''-Al$_2$O$_3$ electrolyte to inactive α-Al$_2$O$_3$ represents a key issue of the energy storage systems. Na-based batteries require hermetic and corrosion resistant seals to provide containment for the molten materials and electrical insulation between the battery case and cathode [9]. A reliable sealant between the β''-Al$_2$O$_3$ tube and the α-Al$_2$O$_3$ collar is necessary and needed for both safety and performance reasons [10].

Glass and glass-ceramics are usually employed to seal the ceramic constituents of the ZEBRA cell because the glass sealing is considered

**Table 1**
Composition in wt% of G018-402 glass and ABB glass.

| Composition | G018-402 glass (wt%) [24] | ABB glass (wt%) |
|---|---|---|
| SiO$_2$ | 40–50 | – |
| B$_2$O$_3$ | >25-30 | 57–60 |
| Al$_2$O3 | 17–25 | 6–8 |
| Na$_2$O | 5–15 | – |
| MO (MgO + CaO + SrO + BaO) | <2 | 33-36 (only BaO) |
| Others (ZnO + TiO$_2$ +SnO$_2$) | 0–5 | – |

**Table 2**
Glass systems used to join α-Al$_2$O$_3$ collar to the β''-Al$_2$O$_3$ tube.

| Glass | G018-402 (wt%) | ABB (wt %) | Al$_2$O$_3$ (wt %) | Li$_2$CO$_3$ (wt %) | Na$_2$CO$_3$ (wt %) |
|---|---|---|---|---|---|
| GA | 75 | – | 25 | – | – |
| GAL | 74 | – | 24 | 2 | – |
| GAN | 74 | – | 24 | – | 2 |
| ABB | – | 100 | – | – | – |
| ABB+Al$_2$O$_3$ | – | 75 | 25 | – | – |

one of the most reliable technologies to ensure the safety and good performance of the device [11]. Glass-based sealants are attractive due to the versatility of glass manufacturing and sealing processing strategies, as well as the possibility of tailoring the properties by compositional design [9,12]. Due to the hostile environment in which these devices operate, the design and selection of appropriate sealing compositions can be challenging [13,14]. Furthermore, the glass sealants must have an adequate coefficient of thermal expansion (CTE) to minimize the thermal stresses and appropriate characteristic temperatures, thus exhibiting simultaneously adhesion with α- and β''-alumina, thermal and chemical stability.

Previous research has indicated that the addition of sodium oxide and alkaline earth oxides, such as CaO, SrO or BaO, can increase the corrosion resistance of aluminoborate [15,16] and aluminoborosilicate glasses [17]. It has been observed that the aluminoborosilicate glasses are susceptible to corrosion in molten sodium and its vapour, while they are resistant to sulphur corrosion. On the other hand, aluminoborate glasses showed the opposite behaviour, resisting to molten sodium and its vapour. Furthermore, it was reported in Ref. [18] that the addition of alumina improves the corrosion resistance to molten sodium salts and alumina is the ceramic used in the ZEBRA battery due to its excellent corrosion resistance. Furthermore, the partial substitution of SiO$_2$ with Bi$_2$O$_3$ has been found to improve the thermal expansion match between the glass sealant and alumina substrates, as well as increase the glass transition temperature (T$_g$), the softening temperature (T$_d$) and the viscosity of the doped glass [10,19]. The same authors have reported satisfying chemical stability of glass-ceramics sealants [20] produced from the parent glasses with a similar composition to those studied in Ref. [19].

Smeacetto et al. have reported good corrosion resistance of a borosilicate glass in molten sodium at 300 °C for 250 h, following a sealing thermal treatment at 1100 °C to join α- to β''-Al$_2$O$_3$ [21]. Other studies [16,18,22] have highlighted that the presence of a high quantity of silicon dioxide in a sodium battery can induce or accelerate sodium corrosion, leading to the undesirable formation of crystalline sodium metasilicate and silicon [18]. To address this issue, Megerle et al. have reported silica-free compositions, including a sodium borate-based glass containing Cs$_2$O and alkaline earth aluminoborate compositions [23], specifically designed for sodium-sulphur battery applications operating at temperatures between 300 and 400 °C.

In this work, the process to produce a new sodium-zinc solid-electrolyte battery was studied by selecting and modifying a commercial silica-based sodium resistant glass. Furthermore, the composition of a new silica-free glass was designed and optimised to further reduce the sealing temperature and, consequently, minimize the manufacturing process costs associated with the new battery.

## 2. Experimental procedure

Two different glass-based systems were studied to seal the ceramic components (α-Al$_2$O$_3$ collar and the β''-Al$_2$O$_3$ tube) of a Na–Zn solid-electrolyte cell: (i) an alumina-modified commercial silica-based glass, selected for its high Na-corrosion resistance and (ii) an original silica-free glass with low sealing temperature. α-Al$_2$O$_3$ and β''-Al$_2$O$_3$ ceramic components were produced by FZSoNick SA company starting from
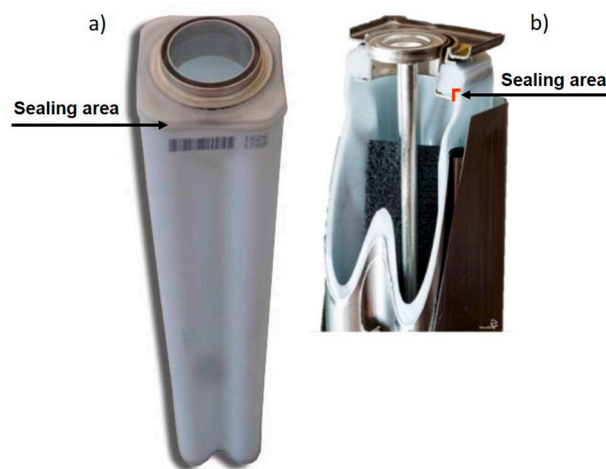


**Fig. 1.** Single solid-electrolyte cell produced by the FZSoNick SA company [4]: (a) front-view and (b) cross-section in which the sealing area between the α-Al$_2$O$_3$ collar and the β''-Al$_2$O$_3$ solid-electrolyte tube is indicated by the black arrow.

Boehmite raw material by calcination and isostatic pressing of 50–80 μm (D50) sized powders, which subsequently were sintered at high temperature (processing is covered by trade secret). The commercial glass (G018-402) used in this study was specifically developed by SCHOTT AG (Landshut, Germany) for the hermetic sealing and joining of ceramics and/or metals in highly corrosive environments, such as molten sodium batteries. The glass composition is shown in Table 1 [24]. To enhance the Na corrosion resistance, alumina microfine powder (>99.5 % purity, with a grain size distribution of D50 = 3 μm) was added to the sealing glass. Additionally, alkaline carbonates, namely Na$_2$CO$_3$(Sigma Aldrich, ≥99.5 % purity) and Li$_2$CO$_3$ (Sigma Aldrich, 99.99 % purity), were added to modify the contact angle on alumina substrates at the sealing temperature. The specific proportions are shown in Table 2. Furthermore, a new silica-free Al$_2$O$_3$–B$_2$O$_3$–BaO glass system (referred to as ABB), was developed with the support of the SciGlass® software (Science Serve GmbH, Sciglass 6.6 software, Newton, Massachusetts, USA). The ABB composition is reported in Table 1. This glass was produced by conventional melting and casting techniques using high-purity grade raw materials: B$_2$O$_3$(precursor H$_3$BO$_3$, Sigma Aldrich, 99 % purity), Al$_2$O$_3$ (Alfa Aesar, 99.9 % purity) and BaO (precursor Ba$_2$CO$_3$ Thermoscientific, 99.8 % purity). The raw material powders were mixed for 24 h and then melted in a Pt–Rh crucible using an electric furnace (LHT418PN2, Nabertherm GmbH, Lilienthal/Bremen, Germany) in air at 1350 °C for 1 h (with a lid covering the crucible) and then at 1400 °C for 30 min (without lid). Subsequently, the melt was cast onto a metal plate, ball-milled, and sieved to obtain a particle size <38 μm. Additionally, alumina microfine powder was added in the proportions reported in Table 2, to potentially improve the Na corrosion resistance.

In both the glass systems, the powders were mixed with a laboratory roller mixer for 24 h after the addition of Al$_2$O$_3$, Li$_2$CO$_3$, and/or Na$_2$CO$_3$.

All the glass powders were thermally characterised by means of the hot stage microscopy (HSM; Hesse Heating Microscope, Germany), from
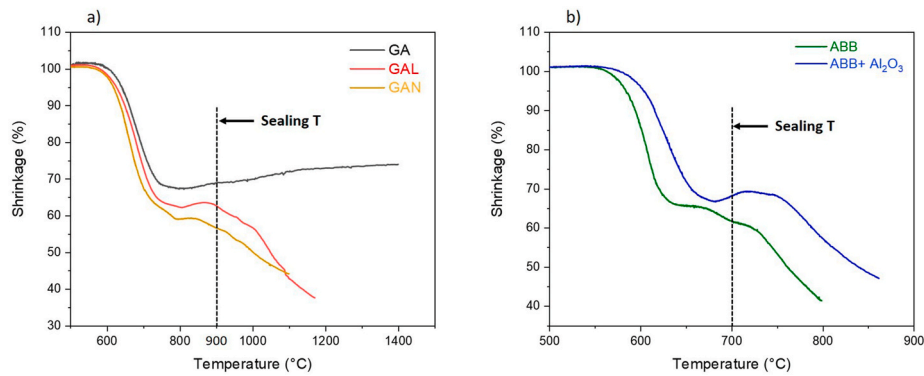
**Fig. 2.** HSM curves of (a) GA, GAL and GAN and (b) ABB, ABB+Al$_2$O$_3$ glass-based sealants; all the analyses were carried out at 5 °C/min heating rate, from room temperature up to the flow temperature detected by the instrument. The black arrow indicates the selected sealing temperature for each glass-based system. ..

| Samples | T$_{fs}$ | T$_{ms}$ | DT | ST | HT | FT | Dwell start | Dwell end |
|---|---|---|---|---|---|---|---|---|
| GA | T= 614°C | T= 790°C | T= 886°C | T= 1269°C | | | T= 900°C | T= 900°C |
| GAL | T= 584°C | T= 765°C | T= 807°C | T= 903°C | T= 1043°C | T= 1161°C | T= 900°C | T= 900°C |
| GAN | T= 581°C | T= 745°C | T= 789°C | T= 868°C | T= 966°C | T= 1090°C | T= 900°C | T= 900°C |
| ABB | T= 580°C | T= 630°C | T= 649°C | T= 681°C | T= 751°C | T= 790°C | T= 700°C | T= 700°C |
| ABB+Al$_2$O$_3$ | T= 597°C | T= 668°C | T= 696°C | T= 719°C | T= 774°C | T= 852°C | T= 700°C | T= 700°C |

**Fig. 3.** Images of characteristic temperatures detected by the hot stage microscope during heating from room temperature to the flow temperature (T$_{fs}$, T$_{ms}$, DT, ST, HT, FT). The images at the dwell start and dwell end show the modification of the sample shape during the dwelling at the chosen sealing temperature: 900 °C for 40 min for G018-402-based systems and 700 °C for 1 h for ABB-based systems.

room temperature up to the melting point identified by the instrument, with a heating rate of 5 °C/min. The sintering behaviour of a compact of glass powders was investigated on Al$_2$O$_3$ plates. Furthermore, the same analyses were carried out with HSM to study the contact angle variation during time at the sealing temperature.

Based on the results obtained from the HSM analyses, α-Al$_2$O$_3$/sealant/β''-Al$_2$O$_3$ samples were produced using the investigated glass-based sealants. A slurry paste composed of water (approximately 40 wt%) and powders (approximately 60 wt%) was manually deposited with a syringe between the α-Al$_2$O$_3$ collar and the β''-Al$_2$O$_3$ tube (Fig. 1a) to be joined; for ABB-based system, ethanol was used instead of water. Subsequently, the samples were subjected to the sealing thermal treatment at 900 °C for 40 min (for the G018-402-based system) or 700 °C for 1 h (for the ABB-based system). All of these treatments were carried out at a heating rate of 5 °C/min under flowing N$_2$–H$_2$ (95 vol %-5vol%). The inert atmosphere was necessary to prevent oxidation of the nickel current collector present in the tubular cell.

Furthermore, some of the sealed samples were cross-sectioned and prepared for scanning electron microscopy (SEM) and energy-dispersive spectrometer (EDS) characterisation. A field-emission scanning electron microscope (FE-SEM, Merlin electron microscope, ZEISS, Oberkochen,

Germany) equipped with an energy-dispersive spectrometer (EDS) (EDS, Zeiss Supra TM 40, Oberkochen, Germany), was used to morphologically investigate α- and β''-Al2O3/sealant interfaces and to analyse the composition of the joining layer. Before SEM investigation, the cross-sectioned samples were polished using SiC papers (grit size 120–4000) and then coated with Pt. The thermal expansion coefficient (CTE), the glass transition temperature (T$_g$) and the dilatometric softening temperature (T$_d$) of the different glass-based systems, after the thermal treatment used for the sealing process, were determined by dilatometry (Netzsch DIL 402 PC) using a heating rate of 5 °C/min. X-ray diffraction (XRD) analyses were carried out on the glass-based sealants obtained after the sealing thermal treatment. The measurements were conducted between 10° and 70° using a X'Pert Pro MRD diffractometer with Cu Kα radiation (PANalytical X'Pert Pro, Philips, Almelo, The Netherlands), with the aid of the X-Pert HighScore software; the crystalline phases were identified using JCPDS database provided by ICDD (International Centre for Diffraction Data, Newton Square, Pennsylvania, USA).

## 3. Results and discussion

Thermal and thermo-mechanical properties of the different glass-

**Table 3**

Equations and R-square values obtained through fitting the characteristic fixed viscosity points and related temperatures of G018-402-based systems (GA, GAL, GAN) and ABB-based systems (ABB, ABB+Al$_2$O$_3$) studied to join α-Al$_2$O$_3$ collar and the β''-Al$_2$O$_3$ tube.

| Glass | equation | R-square |
|---|---|---|
| GA | $y = 4126.33035x^{-0.95113}$ | 0.9682 |
| GAL | $y = 42570.35264x^{-1.31883}$ | 0.9252 |
| GAN | $y = 97139.66842x^{-1.44920}$ | 0.9179 |
| ABB | $y = 6.15585x^{-3.19168}$ | 0.9770 |
| ABB+Al$_2$O$_3$ | $y = 6.66612x^{-2.82669}$ | 0.9481 |

based systems, whose compositions are indicated in Table 2, were investigated. The sintering behaviour of the G018-402 silica-based system (Fig. 2a) and the ABB silica-free system (Fig. 2b) was analysed using hot stage microscopy (HSM). The graphs show the linear shrinkage plotted against the temperature, from room temperature to the flow point identified by the instrument. Furthermore, Fig. 3 illustrates the main characteristic temperatures detected during the HSM analyses: (i) $T_{fs}$ and (ii) $T_{ms}$, which are the first two characteristic points at which linear shrinkage of the glass starts and assumes the maximum value, respectively; (iii) DT, the temperature at which the first signs of softening are observed; (iv) the sphere temperature (ST), which is the point detected where the height of the sample is equal to the width of the base; (v) the half-ball point (HT), which is the temperature at which the height of the sample is half the width of the base and (vi) flow temperature (FT), the temperature at which the height of the sample drops to below one-third of the base [25].

It is evident in Fig. 2a that in the G018-402 silica-based system, the

initial shrinkage, primarily determined by the glass matrix, is minimally influenced by the presence of Li$_2$CO$_3$ and Na$_2$CO$_3$ additives. However, a different behaviour can be observed after the onset of the sintering. In particular, the addition of alkaline carbonates led to lower characteristic temperatures and improved the wettability, especially for the GAN sample.

In the case of the ABB silica-free system (Fig. 2b), when alumina is added to the ABB glass matrix (ABB+Al$_2$O$_3$ sample), a delay in terms of deformation temperature is observed. This delay can be attributed to the increased viscosity resulting from the addition of Al$_2$O$_3$, which hinders further shrinkage through viscous flow. Consequently, the characteristic temperatures of the ABB+Al$_2$O$_3$ sample after the onset of the sintering show a significant shift of some tens of degrees compared to the parent ABB glass.

The method proposed by M. J. Pascual et al. [25] was adopted to predict the viscosity vs T behaviour of the glass-based sealants at fixed viscosity points. In all cases, experimental viscosity points were fitted calculating the constants of the equation $y = ax^b$ and the R-square values (reported in Table 3) by non-linear regression, fitting the experimental characteristic figures with Log η < 10. Fig. 4 shows the results obtained by plotting the characteristic temperatures of the G018-402 silica-based system (Fig. 4a) and of the ABB silica-free one (Fig. 4b), along with trend lines used to predict the viscosity of both systems as a function of temperature. At a temperature of around 900 °C, the GA, GAL and GAN glasses exhibited viscosity values of approximately $10^{6.5}$, $10^{5.4}$ and $10^{5.1}$ Pa·s, respectively, while the ABB and ABB+Al$_2$O$_3$ glasses exhibited viscosity values of approximately $10^{5.1}$ Pa·s and $10^6$ Pa·s, respectively at 700 °C. By predicting the viscosity of the glass-based systems at different temperatures, the trend lines in Fig. 4 assist in optimizing the
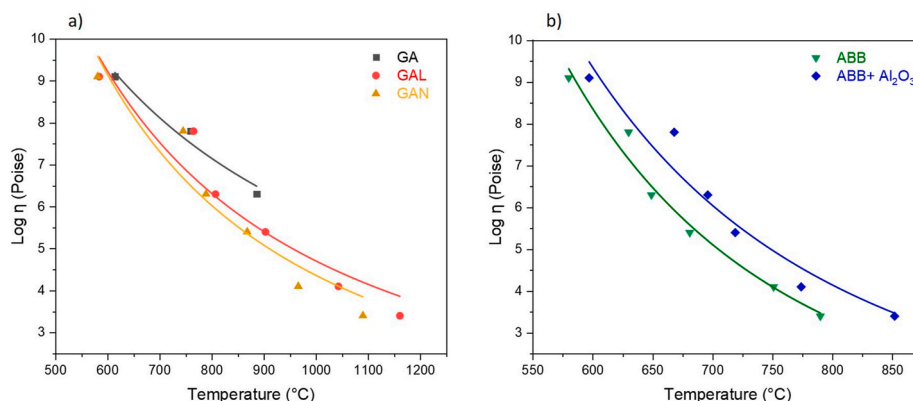


**Fig. 4.** Log η vs Temperature curves for (a) the G018-402-based systems and (b) the ABB-based systems obtained by fitting the characteristic fixed viscosity points and related temperatures [25], calculating.
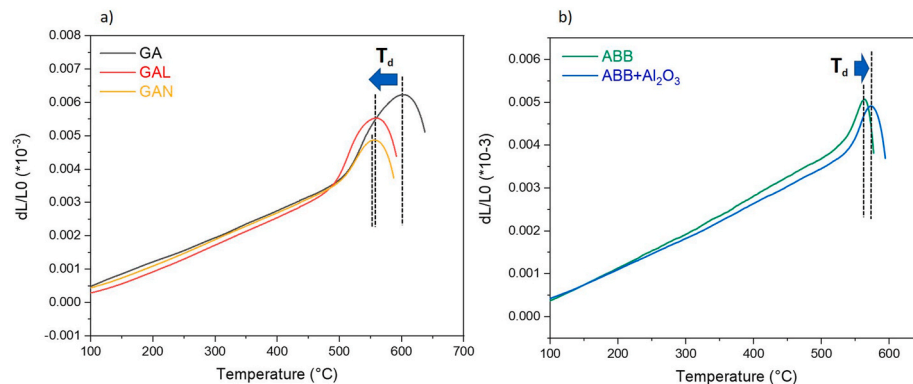


**Fig. 5.** Dilatometry curves of (a) GA, GAL and GAN and (b) ABB, ABB+Al$_2$O$_3$ obtained after sintering at 900 °C for 40 min and 700 °C for 1 h, respectively; all the analyses were carried out with a heating rate of 5 °C/min.

**Table 4**
Glass transition temperature ($T_g$), dilatometric softening temperature ($T_d$) and coefficient of thermal expansion (CTE) of G018-402- and ABB-based systems.

| Glass after sealing process | $T_g$ (°C) | $T_d$ (°C) | CTE ($\cdot 10^{-6}$ K$^{-1}$) | Sealing process |
|---|---|---|---|---|
| | | | (100–300 °C) | (T, time) |
| GA | 511 | 603 | 7.3 | 900 °C, 40 min |
| GAL | 492 | 559 | 7.2 | 900 °C, 40 min |
| GAN | 502 | 555 | 7.2 | 900 °C, 40 min |
| ABB | 537 | 564 | 7.6 | 700 °C, 1 h |
| ABB+Al$_2$O$_3$ | 544 | 574 | 7 | 700 °C, 1 h |

manufacturing process, enabling the achievement of desired glass flow and successful bonding with the alumina substrates.

Based on the HSM results, the following sealing heat treatments were proposed: 900 °C for 40 min (for the G018-402-based systems) and 700 °C for 1 h (for the ABB-based systems), both with a heating rate of 5 °C/min and under flowing N$_2$–H$_2$ (95 vol%-5vol%).

To simulate the chosen sealing process, HSM analyses were conducted on all the glass systems. The analyses involved heating the samples from room temperature up to the proposed sealing temperature, with the specified dwelling time. The images at the beginning and end of the dwelling period at the selected sealing temperature are reported in Fig. 3. The observed modifications in the samples' shape during the

dwelling period provide valuable insights. In the case of G018-402, the addition of Li$_2$CO$_3$ and Na$_2$CO$_3$, even if in low amount (2 wt%), resulted in the incorporation of the alkaline oxides in the glass network, after their decomposition (T ~ 730 °C for Li$_2$CO$_3$ [26] and T ~ 860 °C for Na$_2$CO$_3$ [27]). As a result, the viscosity of the glass decreased and the wettability of the glass on alumina improved. On the other hand, in the ABB glass system, the addition of 25 wt% of alumina to the ABB glass resulted in a delay in the characteristic temperatures. The half-sphere shape was reached at 681 °C for the ABB glass, whereas the ABB+Al$_2$O$_3$ sample achieved the sphere shape only during the dwelling time. It is worth noting that, as expected, the ABB and ABB+Al$_2$O$_3$ contact angles decreased during the dwelling at the sealing temperature, but the presence of alumina reduced the wettability. The coefficient of thermal expansion (CTE), the glass transition temperature ($T_g$) and the softening dilatometric temperature ($T_d$) of all the glasses subjected to the sealing processes were measured by means of the dilatometry.

Fig. 5 shows the dilatometric curves obtained using a heating rate of 5 °C/min. As discussed above, the addition of Li$_2$CO$_3$ and Na$_2$CO$_3$ to the G018-402 (Fig. 5a) resulted in a reduction in glass viscosity. Consequently, $T_g$ and $T_d$ decreased with the presence of alkaline carbonates (as shown in Table 4). Additionally, the CTE values slightly decrease from 7.3$\cdot$ 10$^{-6}$ K$^{-1}$ for GA to 7.2$\cdot$ 10$^{-6}$ K$^{-1}$ for both GAL and GAN samples. On the other hand, the addition of 25 wt% of Al$_2$O$_3$ to the ABB glass (Fig. 5b) led to a slightly higher $T_g$ value (from 537 °C in ABB glass to 544 °C in ABB+Al$_2$O$_3$) and $T_d$ (from 564 °C in ABB glass to 574 °C in ABB+Al$_2$O$_3$). All the CTE values measured for the studied sealant systems are similar to the alumina one (7.3$\cdot$ 10$^{-6}$ K$^{-1}$ in the temperature
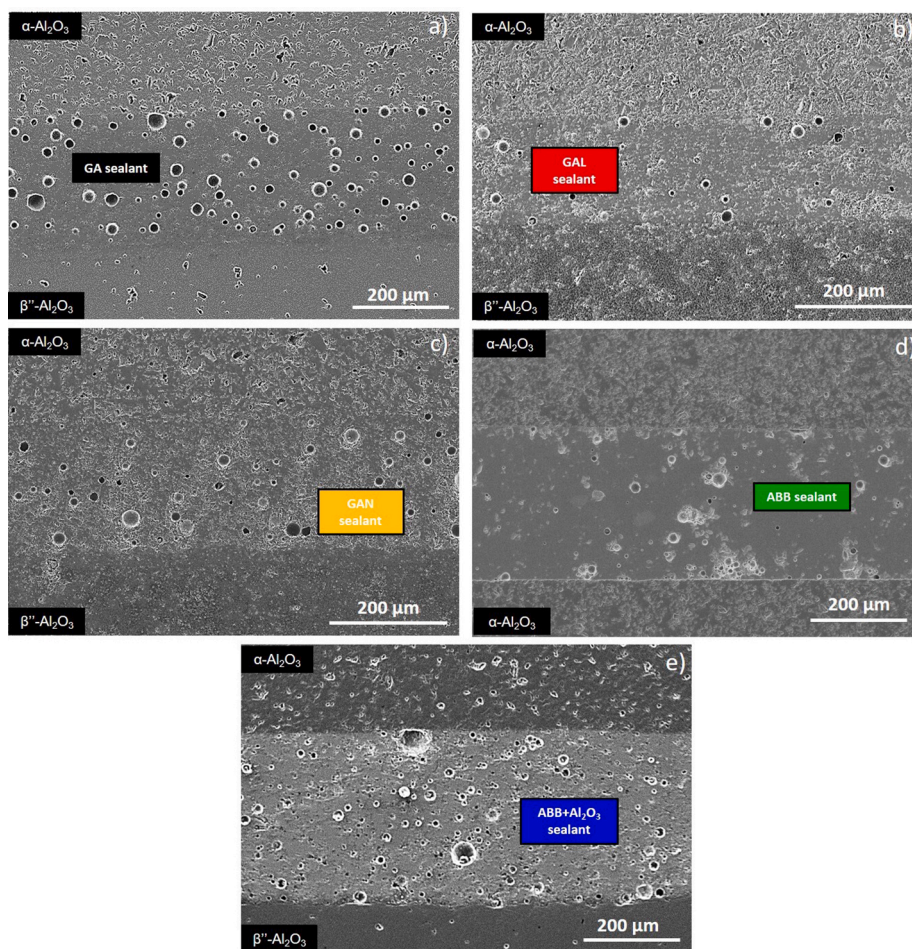


**Fig. 6.** SEM images of the cross-section of: (a) α-Al$_2$O$_3$/GA/β''-Al$_2$O$_3$, (b) α-Al$_2$O$_3$/GAL/β''-Al$_2$O$_3$ and (c) α-Al$_2$O$_3$/GAN/β''-Al$_2$O$_3$ produced at 900 °C for 40 min and (d) α-Al$_2$O$_3$/ABB/β''-Al$_2$O$_3$, (e) α-Al$_2$O$_3$/ABB+Al$_2$O$_3$/β''-Al$_2$O$_3$ produced at 700 °C for 1 h; all the thermal treatments were carried out at 5 °C/min heating rate under flowing N$_2$–H$_2$ (95 vol%-5vol%).
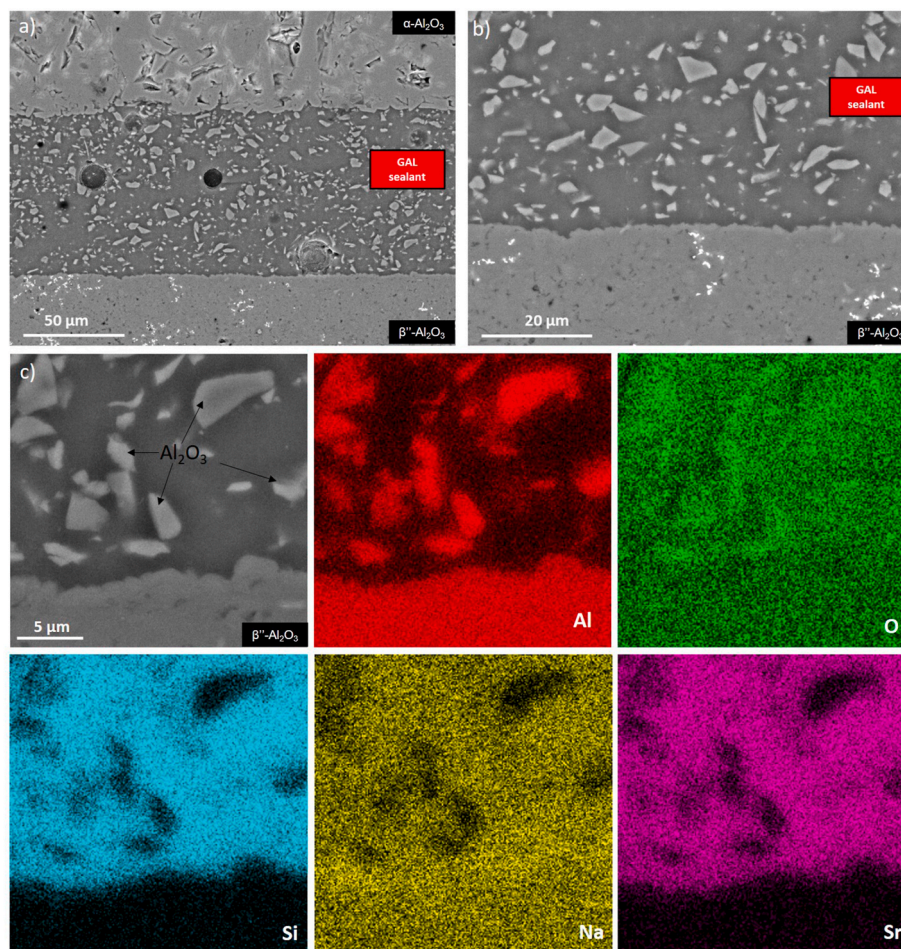
**Fig. 7.** SEM cross-sectional views of (a, b) the $\alpha$-Al$_2$O$_3$/GAL/$\beta$''-Al$_2$O$_3$ joined sample obtained after curing at 900 °C for 40 min and (c) EDS elemental maps of the sealing area; the black arrows indicate alumina particles.

range of 40–300 °C [28]). This similarity suggests that the studied glass-based systems are promising candidate materials for the sealing of $\alpha$-to $\beta$''-Al$_2$O$_3$ components for solid-electrolyte Na–Zn cells.

Fig. 6 shows the cross-section of the $\alpha$-to $\beta$''-Al$_2$O$_3$ joints, obtained after the sealing processes listed in Table 4: $\alpha$-Al$_2$O$_3$/GA/$\beta$''-Al$_2$O$_3$ (a), $\alpha$-Al$_2$O$_3$/GAL/$\beta$''-Al$_2$O$_3$(b), $\alpha$-Al$_2$O$_3$/GAN/$\beta$''-Al$_2$O$_3$ (c), $\alpha$-Al$_2$O$_3$/ABB/ $\beta$''-Al$_2$O$_3$ (d) and Al$_2$O$_3$/ABB+Al$_2$O$_3$/$\beta$''-Al$_2$O$_3$ (e). The thickness of the glass sealant layer ranged from about 200 μm for the G018-402-based systems to around 400 μm for the ABB-based systems; this is reasonable considering the manual deposition used to produce the joints. It is important to note that, despite the manual deposition, in all the samples, the joining layer was continuous, showing good adherence and tightly covered the substrates without visible macroscopic defects. The presence of closed micro-voids is likely due to the manual deposition method used in this preliminary stage to obtain the joined samples. This suggests a following upgrade for considering alternative sealing technologies, such as 3D-printing, to minimize the porosity in the sealing layer.

The glass used to seal $\alpha$-to $\beta$''-Al$_2$O$_3$ components of the solid-electrolyte Na–Zn battery, must fulfil crucial dimensional requirements to fit the battery metallic case [4]. As represented in Fig. 1b, the glass-based sealant has to comply with specific restrictions concerning the sealing area to attain an external dimension of 2–3 mm. Following this criterion, all the studied sealants, apart from GA and ABB (not tested), resulted satisfactory in terms of exhibiting good capillarity and wettability behaviour in joined samples. Additional cross-sectional views, at higher magnification, of $\alpha$-Al$_2$O$_3$/GAL/$\beta$''-Al$_2$O$_3$ and $\alpha$-Al$_2$O$_3$/GAN/$\beta$''-Al$_2$O$_3$ samples can be observed in Fig. 7a,b and

Fig. 8a, respectively. The morphological characterisation confirmed the absence of cracks and defects-free interfaces in both samples, suggesting that no noticeable reactions occur between the glasses and alumina. The sealants are well adhered both to the $\alpha$- Al$_2$O$_3$ and $\beta$''-Al$_2$O$_3$, with no visible delamination phenomena observed at the ceramic/sealant interfaces. The EDS maps (shown in Figs. 7c and 8b) conducted in the sealing area of $\alpha$-Al$_2$O$_3$/GAL/$\beta$''-Al$_2$O$_3$ and $\alpha$-Al$_2$O$_3$/GAN/$\beta$''-Al$_2$O$_3$ samples, revealed the presence of irregularly shaped grains of Al$_2$O$_3$, which were visible in the elemental Al and O maps. These alumina particles were found to be homogeneously distributed in the glass matrix, primarily composed of Si, Na, Al and Sr. No reaction was observed between the alumina particles and the glass matrix in the sealing layer, indicating that the composite structure was maintained after the heat-treatment.

Fig. 9 shows the XRD analysis results of the glass-based sealants after the sealing thermal treatment. The ABB diffractogram exhibited only an amorphous halo, without evidence of crystalline phases. In contrast for GA, GAL, GAN and ABB+Al$_2$O$_3$ samples, along with the amorphous phase, Al$_2$O$_3$ was identified using the PDF card 01-073-1512. These findings align with the microstructural observations presented in Figs. 7 and 8, confirming that no reaction occurred between the alumina powder and the glass matrix within the joining layer.

## 4. Conclusions

In this work, two glass-based systems for sealing $\alpha$- and $\beta$''-Al$_2$O$_3$ in Na–Zn solid-electrolyte cells were studied: a commercial silica-based
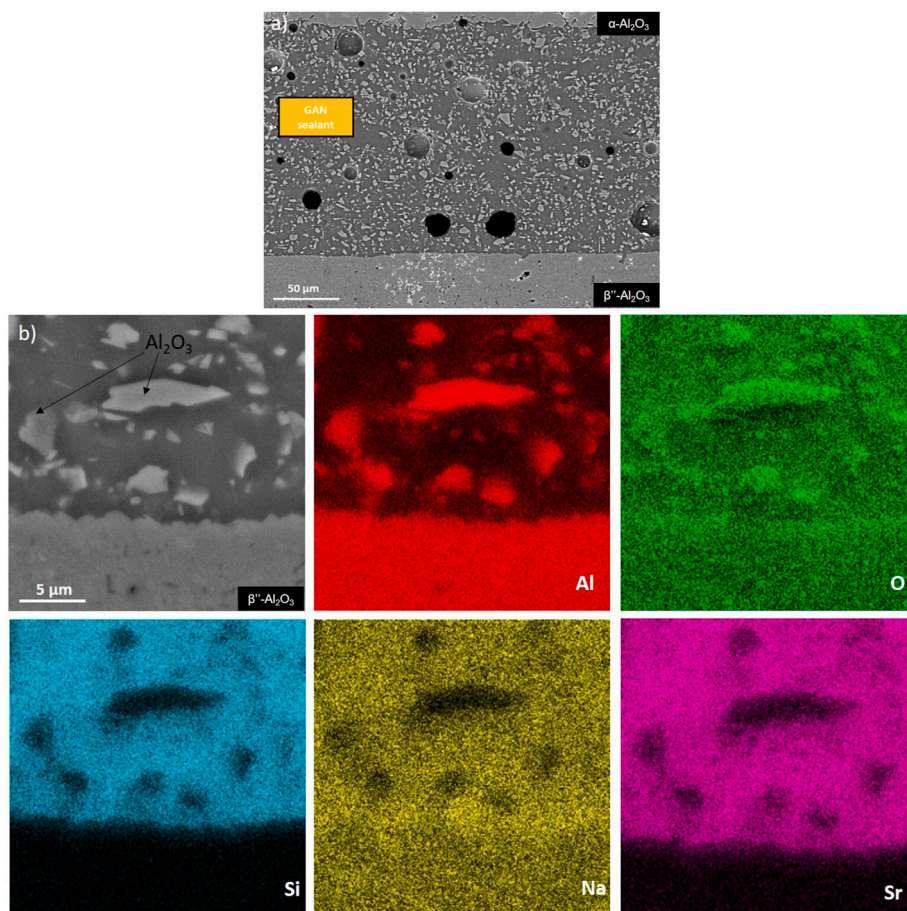
**Fig. 8.** SEM cross-sectional view of (a) the α-Al$_2$O$_3$/GAN/β''-Al$_2$O$_3$ joined sample obtained after curing at 900 °C for 40 min and (b) EDS elemental maps of the sealing area; the black arrows indicate alumina particles.
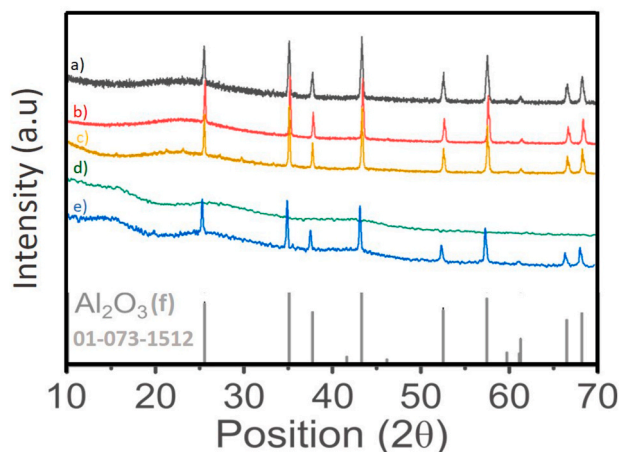


**Fig. 9.** XRD pattern of the following glass sealant candidates: (a) GA, (b) GAL, (c) GAN sintered at 900 °C for 40 min; (d) ABB and (e) ABB+Al$_2$O$_3$ sintered at 700 °C for 1 h. (f) PDF card (number: 01-073-1512) of Al$_2$O$_3$.

glass and a novel silica-free glass system. In both systems, Al$_2$O$_3$ micropowder was added to produce composite materials that could potentially exhibit high resistance to corrosion from molten sodium salts.

Hot stage microscopy analysis revealed that at the chosen sealing temperatures (900 °C for the G018-402 silica-based system and 700 °C for the ABB silica-free system), the wettability and the viscosity of the two systems (~ $10^5$-$10^6$ Poise) are appropriate to guarantee good glass flow and bonding with the alumina components. The incorporation of lithium and sodium carbonates (GAL and GAN samples) led to a lower viscosity and higher wettability on alumina. On the other hand, the alumina addition in the ABB system increased the characteristic temperatures and had the potential to enhance the corrosion resistance against sodium. The CTE values measured for the glass-based sealants ranged from $7 \cdot 10^{-6}$ K$^{-1}$ to $7.6 \cdot 10^{-6}$ K$^{-1}$ within the temperature range of 100–300 °C, which are close to that of Al$_2$O$_3$ ($7.3 \cdot 10^{-6}$ K$^{-1}$) in the same temperature range. Preliminary joined samples were successfully produced with glass-based sealants optimised in this study, and the absence of cracks at the interfaces, in the sealing area and in the alumina substrates, indicates a good thermo-mechanical compatibility between the glass-based sealants and alumina. Furthermore, no reactions were observed in the composite sealing layer between the alumina micro-powder and the glass matrix. These findings show promising results for the application of the studied glass sealants in sodium-based batteries. However, further investigations to optimize the composition and the deposition method will be performed as part of research in this field. Molten sodium salts corrosion tests play a crucial role in assessing the durability of the proposed sealants and the role of the Al$_2$O$_3$ micro-powder addition to the glass sealants. These tests are currently in progress.

## Declaration of competing interest

The authors declare that they have no known competing financial interests or personal relationships that could have appeared to influence the work reported in this paper.

## Acknowledgments

## References

[1] A. Zecca, L. Chiari, Fossil-fuel constraints on global warming, Energy Pol. 38 (2010) 1–3, https://doi.org/10.1016/j.enpol.2009.06.068.

[2] J.L. Sudworth, The sodium/nickel chloride (ZEBRA) battery, J. Power Sources 100 (2001) 149–163, https://doi.org/10.1016/S0378-7753(01)00891-6.

[3] C.H. Dustmann, Advances in ZEBRA batteries, J. Power Sources 127 (2004) 85–92, https://doi.org/10.1016/j.jpowsour.2003.09.039.

[4] R. Benato, N. Cosciani, G. Crugnola, S. Dambone Sessa, G. Lodi, C. Parmeggiani, M. Todeschini, Sodium nickel chloride battery technology for large-scale stationary storage in the high voltage network, J. Power Sources 293 (2015) 127–136, https://doi.org/10.1016/j.jpowsour.2015.05.037.

[5] R. Manzoni, Sodium nickel chloride batteries in transportation applications, Electr. Syst. Aircraft, Railw. Sh. Propulsion, ESARS. (2015) 1–6, https://doi.org/10.1109/ESARS.2015.7101491.

[6] N.E. Holubowitch, S.E. Manek, J. Landon, C.A. Lippert, S.A. Odom, K. Liu, Molten zinc alloys for lower temperature, lower cost liquid metal batteries, Adv. Mater. Technol. 1 (2016) 1–9, https://doi.org/10.1002/admt.201600035.

[7] J. Xu, O.S. Kjos, K.S. Osen, A.M. Martinez, O.E. Kongstein, G.M. Haarberg, Na-Zn liquid metal battery, J. Power Sources 332 (2016) 274–280, https://doi.org/10.1016/j.jpowsour.2016.09.125.

[8] J. Xu, A.M. Martinez, K.S. Osen, O.S. Kjos, O.E. Kongstein, G.M. Haarberg, Electrode behaviors of Na-Zn liquid metal battery, J. Electrochem. Soc. 164 (2017) A2335–A2340, https://doi.org/10.1149/2.0591712jes.

[9] I.W. Donald, P.M. Mallinson, B.L. Metcalfe, L.A. Gerrard, J.A. Fernie, Recent developments in the preparation, characterization and applications of glass- and glass-ceramic-to-metal seals and coatings, J. Mater. Sci. 46 (2011) 1975–2000, https://doi.org/10.1007/s10853-010-5095-y.

[10] S. Song, Z. Wen, Q. Zhang, Y. Liu, A novel Bi-doped borosilicate glass as sealant for sodium sulfur battery. Part 1: thermophysical characteristics and structure, J. Power Sources 195 (2010) 384–388, https://doi.org/10.1016/j.jpowsour.2009.06.041.

[11] Z. Wen, Y. Hu, X. Wu, J. Han, Z. Gu, Main challenges for high performance NAS battery: materials and interfaces, Adv. Funct. Mater. 23 (2013) 1005–1018, https://doi.org/10.1002/adfm.201200473.

[12] A.K. Varshneya, J.C. Mauro, in: Fundamentals of Inorganic Glasses, third ed., 2019. Amsterdam, Netherlands.

[13] S.G. Leonardi, M. Samperi, L. Frusteri, V. Antonucci, C. D'Urso, A review of sodium-metal chloride batteries: materials and cell design, Batteries 9 (2023) 524, https://doi.org/10.3390/batteries9110524.

[14] K. Jung, S. Lee, G. Kim, C.S. Kim, Stress analyses for the glass joints of contemporary sodium sulfur batteries, J. Power Sources 269 (2014) 773–782, https://doi.org/10.1016/j.jpowsour.2014.07.071.

[15] A.J. Burggraaf, H.C. Van Velzen, Glasses resistant to sodium vapor at temperatures to 700°C, J. Am. Ceram. Soc. 52 (1969) 238–242, https://doi.org/10.1111/j.1151-2916.1969.tb09174.x.

[16] A. Herczog, Sodium ion conducting glasses for the sodium-sulfur battery, J. Electrochem. Soc. 132 (1985) 1539–1545, https://doi.org/10.1149/1.2114161.

[17] D.-S. Park, C. Park, L. Navias, US, Sodium Resistant Sealing Glasses, vol. 4, 1981, p. 268, 313.

[18] S. Kumar, D.-S. Park, US, Sealing Glass Composition and Article, vol. 9, 2015, 067,818 B2.

[19] S. Song, Z. Wen, Y. Liu, The effect of substitution of Bi2O3 for alkali oxides on thermal properties, structure and wetting behavior of the borosilicate glass, Mater. Lett. 64 (2010) 1025–1027, https://doi.org/10.1016/j.matlet.2010.01.080.

[20] S. Song, Z. Wen, Y. Liu, J. Lin, X. Xu, Q. Zhang, New glass-ceramic sealants for Na/S battery, J. Solid State Electrochem. 14 (2010) 1735–1740, https://doi.org/10.1007/s10008-010-1028-6.

[21] F. Smeacetto, M. Radaelli, M. Salvo, D. Di Modugno, A.G. Sabato, V. Casalegno, M. Broglia, M. Ferraris, Glass-ceramic joining material for sodium-based battery, Ceram. Int. 43 (2017) 8329–8333, https://doi.org/10.1016/j.ceramint.2017.03.170.

[22] V. Manthina, G. Song, P. Singh, M.K. Mahapatra, Silica-free sealing glass for sodium-beta alumina battery, Int. J. Appl. Ceram. Technol. 16 (2019) 887–895, https://doi.org/10.1111/ijac.13093.

[23] C.A. Megerle, Glass Sealing Materials for Sodium-Sulfur Batteries and Batteries Made Therewith, 1992 EP0503776A1.

[24] https://www.schott.com/en-gb/products/sealing-and-solder-glass-p1000291/downloads (accessed 25 October 2023).

[25] M.J. Pascual, A. Durán, M.O. Prado, A new method for determining fixed viscosity points of glasses, Phys. Chem. Glasses 46 (2005) 512–520.

[26] J.P. Yasnó, S. Conconi, A. Visintin, G. Suárez, Non-isothermal reaction mechanism and kinetic analysis for the synthesis of monoclinic lithium zirconate (m-Li2ZrO3) during solid-state reaction, J. Anal. Sci. Technol. 12 (2021), https://doi.org/10.1186/s40543-021-00267-5.

[27] J.W. Kim, Y.D. Lee, H.G. Lee, Decomposition of Na2CO3 by interaction with SiO2 in mold flux of steel continuous casting, ISIJ Int. 41 (2001) 116–123, https://doi.org/10.2355/isijinternational.41.116.

[28] J. Zygmuntowicz, M. Piatek, A. Miazga, K. Konopka, W. Kaszuwara, Dilatrometric sintering study and characterization of Alumina-nickel composites, Process. Appl. Ceram. 12 (2018) 111–117, https://doi.org/10.2298/pac1802111z.